Electronic Supplementary Material

Detection of Enzyme Activity and Inhibition During Studies in Solution, *In Vitro* and *In Vivo* with CatalyCEST MRI

Journal: Molecular Imaging and Biology

Sanhita Sinharay,[1] Edward A. Randtke,[2] Christine M. Howison,[2]
Natalia A. Ignatenko,[3,4] and Mark D. Pagel[1,2,4]

1. Department of Chemistry and Biochemistry, University of Arizona, Tucson, AZ
2. Department of Medical Imaging, University of Arizona, Tucson, AZ
3. Department of Cellular and Molecular Medicine, University of Arizona, Tucson, AZ
4. University of Arizona Cancer Center, University of Arizona, Tucson, AZ

*Corresponding author's email address: mpagel@u.arizona.edu

1. Chemical Synthesis and Supplies

1.1. General synthesis methods and materials

All reactions were performed under an inert atmosphere of nitrogen or argon using dry solvents unless otherwise indicated (Fig. S1). Flash column chromatography was performed using silica gel (particle size 0.04 - 0.06 mm and 230 - 400 Å mesh size). An analytical HPLC system (600 series pump system with a 2487 dual wavelength UV detector, Waters Corp.) was used for analysis and an octadecyl polymer "Sep Pak" cartridge column (Sigma Aldrich, St. Louis MO) for purification of the final compound. Reactions were monitored using thin layer chromatography (TLC) on silica gel plates (Sigma Aldrich).

1.2. Physical measurements

^{1}H and ^{13}C NMR spectra were recorded with Bruker AVIII 400 MHz, DRX 500 MHz and DRX 600 MHz NMR instruments (Bruker Biospin, Inc., Billerica, MA). High resolution mass spectra were obtained with a Ultraflex III Maldi TOF-TOF instrument (Bruker Daltonics, Inc., Billerica, MA) and LC-MS data were obtained with a UHPLC high throughput analytical LC-MS system.

1.3. Synthesis of compound 1

Compound **1** was synthesized and purified using a reported procedure with 70% yield [8]. ^{1}H NMR (499 MHz, chloroform-d) δ 7.83 (s, 1H), 7.48 (m, 2H). 7.43-7.30 (m, 8H), 6.30-6.27 (m, 3H), 5.33 (s, 2H), 5.14 (s, 2H). LRMS-ESI (m/z): $[M+H]^{+}$ calcd for $[C_{12}H_{21}NO_3]$, 334.1; found, 334.1

1.4. Synthesis of compound 2

Compound **2** was synthesized by modifying a reported procedure [S1]. A solution of Boc-L-dibenzyloxycarbonyl arginine (10.0 g, 18.6 mmol) in 60 mL tetrahydrofuran was treated dropwise with anhydrous pyridine (1.5 mL, 18.6 mmol) and followed by addition of Boc-anhydride (4.05 g, 18.6 mmol) in a 300 mL round-bottom flask, equipped with a magnetic stirrer and under inert N_2, and allowed to stir at room temperature for 1 h. Then a solution of compound **1** (2.0 g, 6.2 mmol) in 60 mL tetrahydrofuran was added to the flask and the reaction

mixture was allowed to stir at room temperature for 16 h. On completion, the reaction mixture was diluted with ethyl acetate (100 mL) and washed with saturated $NaHCO_3$ (15 mL) followed by 1 M HCl (15 mL) and water (15 mL). The final compound was washed with brine (10 mL) and organic layers were extracted with ethyl acetate, dried over Na_2SO_4 and purified by SiO_2 column chromatography (30% to 50% ethyl acetate to hexanes). The final compound **2** was obtained as a yellow solid (5.1 g, 5.9 mmol, 95% yield). ^{1}H NMR (499 MHz, chloroform-d) δ 7.64 (d, 1H), 7.33-7.36 (m, 2H), 7.12- 7.30 (m, 24H), 5.22 (s, 2H), 5.14 (s, 2H), 1.64 (m, 4H), 1.36 (s, 9H). LRMS-ESI (m/z): $[M+H]^+$ calc'd for $[C_{48}H_{51}N_5O_{10}]$, 858.3.1; found, 858.1

1.5. Synthesis of compound 3

Compound **2** (1.0 g, 1.16 mmol) was suspended in dry ether (24 mL), and a solution of concentrated HCl in ethyl acetate (0.5 mL in 4 mL) was added dropwise to the reaction mixture at room temperature. The solution was then allowed to stir for 14 h after which the solvents were removed by rotary evaporation. Ether (20 mL) was further added to the yellow precipitate and stirred for another 2 h. The solvent was then removed by rotary evaporation and the product was purified by flash chromatography over SiO_2 (9:1 dichloromethane:methanol) to yield compound **3** as a yellow oil (0.57 g, 0.75 mmol, 65%). The final compound was analyzed by HPLC (RP C-18, 10-90 0.1%TFA: acetonitrile in 45 min, R_t = 26.21 min) LRMS-ESI (m/z): $[M+H]^+$ calc'd for $[C_{43}H_{44}N_5O_8]$, 758.1; found, 758.1

1.6. Synthesis of compound 4

Z-Phe-OH (0.19 g, 0.65 mmol), (0.29 g, 0.65 mmol) and hydroxybenzotriazole (0.09 g, 0.65 mmol) were added to 30 mL of dimethyl formamide in a 100 mL round-bottom flask with an inert atmosphere and 0□C, followed by the dropwise addition of N-methyl morpholine (0.13 mL, 11.97 mmol) and allowed to equilibrate at 0□C for 15 min. Compound **3** (0.41 g, 0.54 mmol) dissolved in dimethyl formamide (5 mL) was then added to the flask. The ice bath was then removed and the reaction mixture was allowed to stir at room temperature for 8 h. The reaction mixture was then diluted with ethyl acetate (20 mL) and washed with 5% $NaHCO_3$ (2 × 5 mL), 5% citric acid (2 × 5 mL), and water (20 mL). The organic layers were collected, washed with brine (5 mL), and extracted with ethyl acetate (30 mL), and dried over Na_2SO_4. The solvent was removed by rotary evaporation and purified by column chromatography over SiO_2 (9:1 dichloromethane: methanol) to yield the final compound **4** as a yellow oil (0.22 g, 0.21 mmol, 39%). The final compound was analyzed by HPLC (RP C-18, 10-90 0.1%TFA: acetonitrile in 45 min, R_t = 34.47 min). LRMS-ESI (m/z): $[M+H]^+$ calc'd for $[C_{60}H_{59}N_6O_{11}]$, 1039.4; found, 1039.4

1.7. Synthesis of compound 5, FRSA

Compound **4** (0.22 g, 0.21 mmol) was dissolved in 12 mL methanol and 0.1 mL of 1 M HCl in 4 mL ethyl acetate was added to the solution for solubility. A catalytic amount of Pd/C (10% w/w) and $Pd(OH)_2$ (10% w/w) were added to the reaction mixture. The round-bottom flask was then equipped with a H_2 balloon and stirred overnight. The reaction mixture was passed over a fine frit filter with celite and then solvent was removed by rotary evaporation. The final product was purified over a Sep Pak column (water with 0.1% trifluoroacetic acid:acetonitrile) and compound **5** was obtained as a white solid after lyophilization (0.08 g, 0.17 mmol, 83%). The final compound was purified by HPLC (RP C-18, 0-30 0.1%TFA:acetonitrile in 45 min, R_t = 22.1 min). HRMS-ESI (m/z): $[M+H]^+$ calc'd for $[C_{22}H_{29}N_6O_5]$, 457.2199; found, 457.2194

1.8. Other supplies

KLK6 enzyme from a NS0-derived mouse myeloma cell line with a C-terminal 10-His tag was obtained from R&D Biosystems (Minneapolis, MN). Lysyl endopeptidase was purchased from Wako Biochemicals (Richmond, VA). Antithrombin III from human plasma was purchased from Sigma Aldrich (St. Louis, MO).

2. Preparation of samples for CatalyCEST MRI studies *in vitro*

The HCT116 and shKLK6 cell lines were each maintained in Dulbecco's Modified Eagle Medium (DMEM) with 4500 mg/L glucose, L-glutamine without sodium pyruvate, supplemented with 10% FBS and 1% penicillin/ streptomycin and 0.5 mg/ml puromycin (Thermo Fisher Scientific Inc.). Cells were plated in 6-well plates at a concentration of 0.1 x 10^6 cells/well. Conditioned media was collected 48 h after subculture and was centrifuged to remove insoluble materials.

3. Evaluation of CEST MRI conditions

The sample compositions and CEST MRI protocols are described in the Materials and Methods section of the main text.

3.1. The effect of concentration

Samples of the agent were prepared with concentrations ranging from 25 mM to 175 mM. The CEST MR images were acquired with a continuous wave saturation pulse of 4 μT and 5 s of saturation time. A HW-Conc analysis method was used to assess the relationship between concentration and CEST signal amplitude (Fig. 3a) [22]. These linear results were converted to non-linear relationships between CEST signals and concentration (solid lines in Fig. 3b), which matched the experimental results (circles and squares in Fig. 3b). Although the relationship between signal amplitude and concentration is approximately linear at low concentrations, this relationship is clearly non-linear at higher concentrations. Therefore, the HW-Conc analysis method is preferred for calibrating CEST signal amplitudes rather than simply approximating this relationship to be linear.

The average standard deviation of the background noise from one image of our *in vivo* studies was 1.29%. We acquired ten CEST MR images during our *in vivo* study and therefore signal averaging would reduce the standard deviation of noise to 0.40% relative to signal. Assuming the signal to noise ratio is high, the CEST signal has a 95% probability of being real when the CEST signal is greater than 0.40% × 2√2, or 1.16% [17]. The salicylic acid moiety can generate 1.16% CEST signal at 7.0 mM concentration, while the aryl amide can generate this level of CEST signal with 3.8 mM of contrast agent.

3.2. Studies performed with blood plasma.

Blood was drawn from mice bearing a HCT116 tumor, and the supernatant plasma was collected after centrifugation. A total of 100 μL of plasma was added to 30 mM of the contrast agent in 200 μL of Tris buffer at pH 7.3. CEST spectra were obtained in 7.5 minute intervals for 6 hours. The temporal changes in the CEST signal amplitudes were used to determine the reaction coordinate during the time course of the study (Fig. 3c,d). These results indicated a first-order reaction in plasma as expected, showed that the plasma had enzyme activity that could cleave the peptidyl ligand of the agent, and showed that plasma caused some general degradation of the agent. An identical sample was prepared with the addition of 25 μg of Antithrombin III inhibitor and again CEST spectra were collected over 6 hours (Fig. 3e). These results showed no evidence for cleavage of the agent, indicating successful inhibition of relevant enzyme activity in the plasma.

3.3. The effect of saturation time

The same CEST spectra were obtained at saturation times ranging from 0.2 s to 7.0 s using the same sample of 25 mM of agent at 37.0 ± 0.2°C, and with a saturation power of 4 μT (Fig. S3A-C). A RL-QUEST plot was used to assess the dependence of CEST signal on saturation

time (Fig. S3A) [24]. The RL-QUEST analyses were used to create relationships between CEST signal and saturation time for each exchangeable proton (solid lines in Fig. S3B), which matched the experimental results (circles and squares in Fig. S3B). A ratio of these CEST signals derived from the RL-QUEST analysis showed no dependence on saturation time (Fig. S3C). This result agrees with results reported for other CEST agents [8]. The RL-QUEST method was not used to determine chemical exchange rates because this method requires a high concentration of agent for accurate measurements.

3.4. The effect of saturation power

To optimize CEST MRI parameters for subsequent studies, CEST spectra were acquired with a 25 mM solution of the agent in Tris-base buffer (pH 7.3) at saturation powers ranging from 2.0 μT to 7.0 μT and using a saturation time of 5 s and temperature of 37.0 ± 0.2 °C (Fig. S3D-F). A HW-QUESP analysis method was used to determine the chemical exchange rates of the contrast agent before KLK6 catalysis (Fig. 3D) [25]. The HW-QUESP analyses were used to create relationships between CEST signal and saturation power for each exchangeable proton (solid lines in Fig. 3E), which matched the experimental results (circles and squares in Fig. 3E). This linear analysis method has been shown to more accurately measure chemical exchange rates relative to the non-linear QUESP analysis method or the linear LB-QUESP method (also known as the omega plot method) because the HW-QUESP method compensates for inaccurate saturation powers caused by B_1 inhomogeneities.

To assess the effects of incomplete saturation on the reaction coordinate, we compared the reaction coordinate that would be determined with lower saturation powers relative to the highest saturation power used in our study, which was 7.0 μT. The fitted relationships between CEST and saturation power were used to determine the ratio of CEST signals and the reaction coordinate as a function of saturation power from 0 to 7.0 μT. A plot of saturation power vs. the reaction coordinate normalized to the value at 7.0 μT showed that incomplete saturation can lead to underestimating the reaction coordinate and the assessment of enzyme activity (Fig. S3F). This result is intuitive, because very low saturation power will result in very low CEST signal amplitudes that are similar in magnitude (left side of Fig. S3E), so that the ratio of these CEST signals will result in a low reaction coordinate; higher saturation powers allow each CEST signal to “grow” to their maximum magnitude that have different values (right side of Fig. S3E), which results in a determination of a higher reaction coordinate.

The salicylic acid moiety has a two-step exchange mechanism rather than a single-step mechanism used by most CEST agents [8, S2]. This causes the salicylic acid moiety to reach maximum CEST signal at much higher saturation powers than predicted by a theory that is based on a single-step mechanism. Therefore, the dependence of the CEST signal ratio on saturation power is a unique characteristic of CEST agents with a salicylic acid moiety.

3.5. The effect of temperature

To study the effects of temperature on the both CEST signals, 25 mM samples of the agent were prepared at pH 7.3 and CEST spectra were collected with a saturation power of 4 μT and a saturation time of 5 s at temperatures ranging from 22 to 52°C (Fig. S4A). A line was fit to the CEST signals vs. temperature (solid lines in Fig. S4A).

To assess the effects of temperature on the reaction coordinate, the fitted relationships between CEST and temperature were used to determine the ratio of CEST signals and the reaction coordinate as a function of temperature (Fig. S4B). This relationship shows that the reaction coordinate is dependent on temperature. The reaction coordinate varies by 3.2% per °C. Considering that sub-surface tissues have highly consistent temperatures, the effect of temperature on the *in vivo* reaction coordinate is minor.

The chemical exchange rate of the aryl amide should increase exponentially with increasing temperature according to the Arrhenius equation, although this exponential relationship can be approximated to be linear over the tested temperature range. As expected, the CEST signal at 5.3 ppm increased linearly with increasing temperature, (Fig. S4). Conversely, the chemical exchange rate of the salicylic acid moiety decreased with temperature. This non-Arrhenius behavior is attributed to the two-step exchange mechanism between salicylic acid and water, whereby the second step is entropically disfavored relative to the first step [8, S2].

3.6. The effect of pH on catalyCEST MRI

To study the effect of pH on both CEST signals, 25 mM samples of the agent were prepared with pH values ranging from 6.2 to 7.4 and CEST spectra were collected with a saturation power of 3 μT and a saturation time of 5 s. The CEST signal of salicylic acid increased with increasing pH, indicating that the chemical exchange of this moiety is base-catalyzed (Fig. S5a). The CEST signal of the aryl amide moiety was relatively insensitive to changes in pH. Although this amide moiety also has a chemical exchange mechanism that is base-catalyzed, an increase in chemical exchange rate at higher pH values approaches the chemical shift difference between this proton and water (4.2 ppm at 300 MHz magnetic field strength, or 1,260 Hz), which lowers the CEST signal at these higher pH values, an effect known as MR coalescence. This effect is not as strong for the salicylic acid moiety, which has a high chemical shift relative to water (9.8 ppm at 300 MHz magnetic field strength, or 2,940 Hz).

To assess the effects of pH on the reaction coordinate, a line was fit to the CEST signals vs. pH values. The ratio of these fitted lines was used to determine the reaction coordinate at each pH value. A plot of pH vs. the reaction coordinate normalized to the value at pH 7.4 showed that lower pH values can lead to underestimating the reaction coordinate and the assessment of enzyme activity (Fig. S5b). This underestimation may be significant for tumor tissues, which are known to be acidic due to the Warburg effect [29, S3].

4. *in vivo* catalyCEST MRI

4.1. Preparation of the tumor model

To prepare the mouse models, male SCID mice that were 6 to 8 weeks in age were subcutaneously injected in the right rear flank with 1×10^6 to 2×10^6 tumor cells suspended in 150 μL of saline. Imaging studies were conducted 20 days after cell inoculation, when tumors reached approximately 300 mm^3 in diameter. Each mouse was anesthetized with 1.5-2.5% isoflurane delivered in 1 L/min oxygen gas ventilation. The mouse was then secured to a customized MRI–compatible cradle, probes for monitoring rectal temperature and respiration were connected to the mouse, and core body temperature was regulated at 37.0 ± 0.2°C using an automated feedback loop between the temperature probe and an air heater (SA instruments, Inc., Stony Brook, NY).

4.2. *in vivo* catalyCEST MRI results

The results of all *in vivo* catalyCEST MRI studies are shown in Figures S6 and S7.

References

S1. Haftchenary S, et al. (2013) Potent targeting of the STAT3 protein in brain cancer stem cells: a promising route for treating glioblastoma. *ACS Med Chem Lett* 4(11):1102-1107.

S2. Revell LE, Williamson BE (2013) Why are some reactions slower at higher temperatures? *J Chem Educ* 90(8):1024-1027.

S3. Warburg O (1956) On the origin of cancer cells. *Science* 123(3191):309-314.

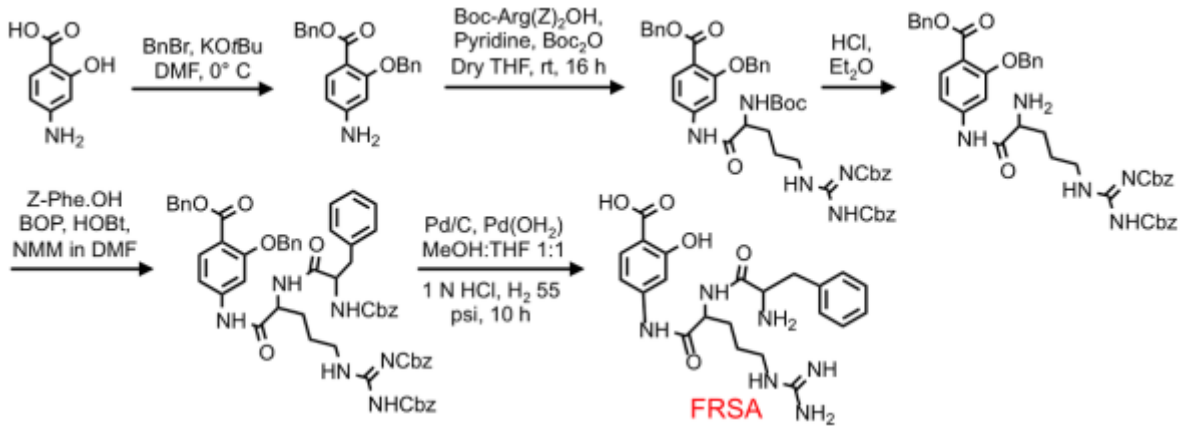

Fig. S1. Chemical synthesis of the contrast agent, FRSA. The synthesis was performed using a modification of a previously reported procedure [8]. The overall yield was 20.0% after HPLC purification.

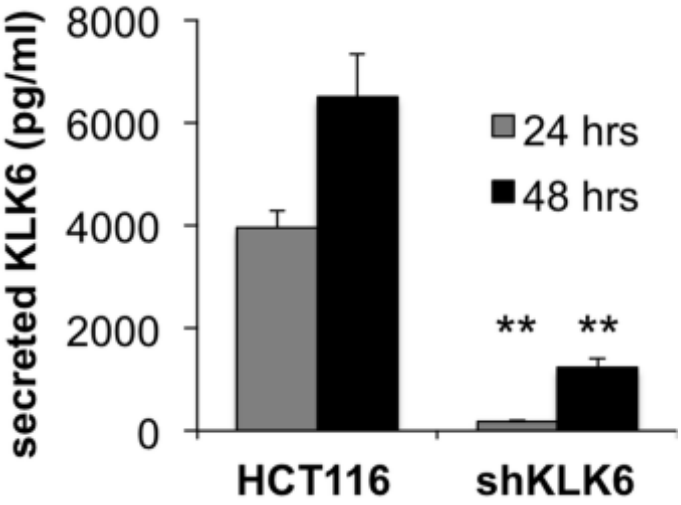

Fig. S2. The concentrations of KLK6 enzyme in conditioned media. HCT116 cells of human colon cancer were tested, as well as HCT116 cells transfected with KLK6 specific small hairpin RNA (shKLK6). Cells were plated at 0.1×10^6 cells/well in triplicate. The conditioned media was collected at the 24 h and 48 h after subculture and KLK6 concentration was determined using a KLK6 ELISA kit. ** $P < 0.01$ when comparing HCT116 vs. shKLK6.

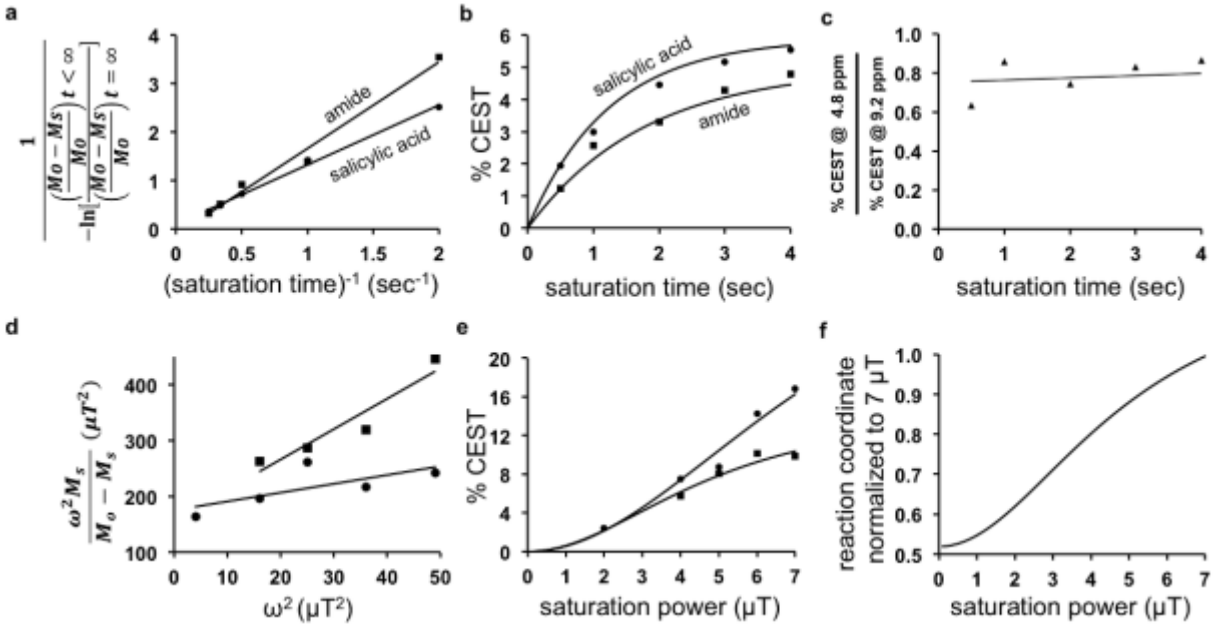

Fig. S3. The effect of saturation time and power on CEST signals. **a** A linear RL-QUEST analysis method was used to fit the relationship between CEST signal vs. saturation time [25]. **b** This linear fitting was then converted to show the relationship between CEST signal vs. saturation time, which matched the experimental results for both the amide and salicylic acid moieties. **c** The ratio of the two CEST signals was relatively insensitive to the saturation time. **d** A linear HW-QUESP analysis method was used to fit the relationship between CEST signal vs. saturation power [15]. **e** This linear fitting was then converted to show the relationship between CEST signal vs. saturation power, which matched the experimental results for both the amide and salicylic acid moieties. **f** The reaction coordinate values were determined as a function of saturation power, which were then normalized to the reaction coordinate value at 7 μT, and then plotted with respect to saturation time. These results demonstrate that incomplete saturation will cause an underestimation of the reaction coordinate.

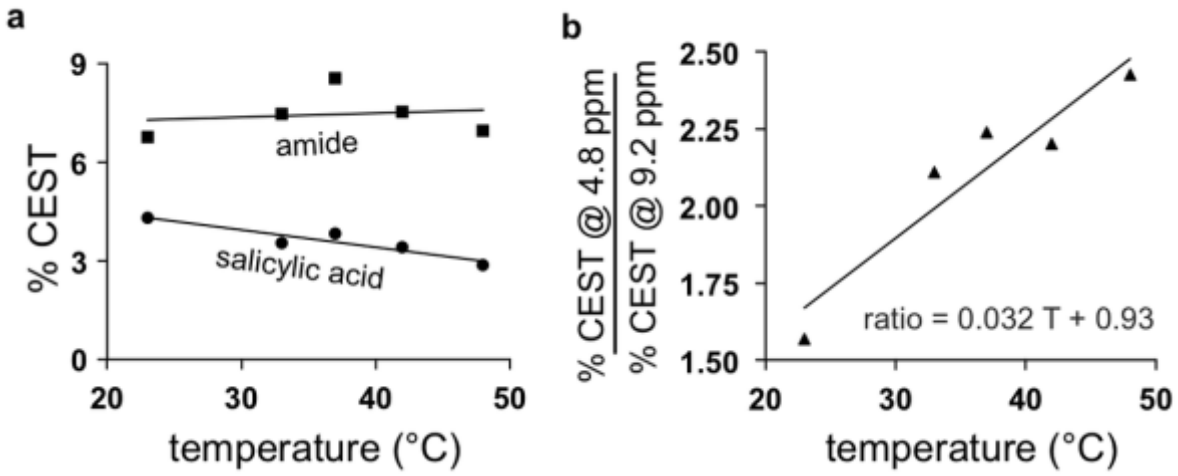

Fig. S4. The dependence of CEST on temperature. **a** The CEST signal amplitude was measured over a range of 23.0 to 48.0°C for the amide and salicylic acid moieties. **b** The ratio of these CEST signal amplitudes was dependent on temperature. A change of 1.0°C from a physiological temperature of 37.0°C would result in a 3.2% change in the CEST ratio, indicating that temperature has a minor effect on the determination of the reaction coordinate that evaluates enzyme activity.

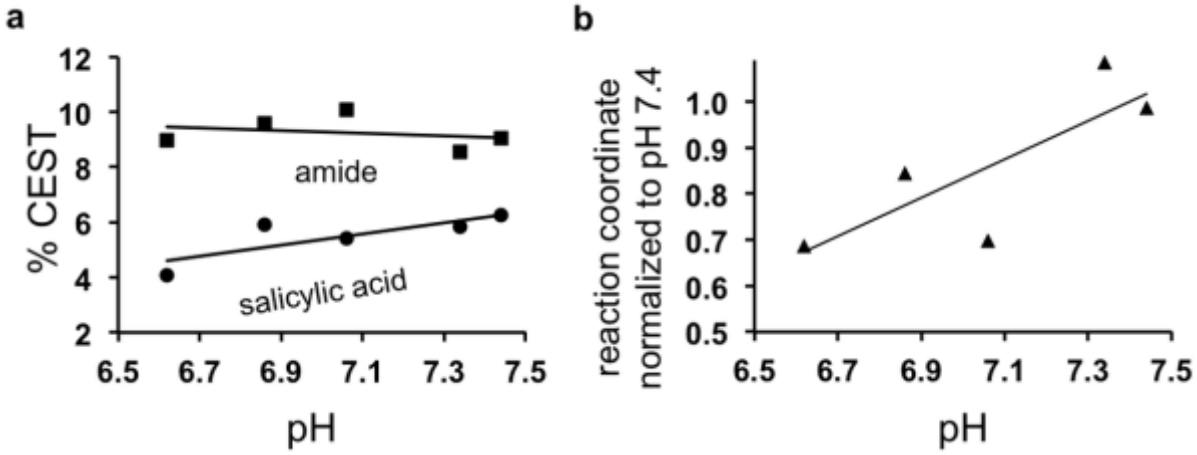

Fig. S5. The dependence of CEST on pH. **a** The CEST signal amplitude was measured over a range of 6.62 to 7.44 pH units for the amide and salicylic acid moieties. A line was fit to each set of experimental results to show the increase in CEST signal from salicylic acid with increasing pH, and the relatively invariant change in CEST signal from the amide with increasing pH. **d** The ratio of the CEST signal amplitudes was used to determine a reaction coordinate. These reaction coordinate values were normalized to the reaction coordinate value at pH 7.4, and then plotted with respect to pH. These results demonstrate that an acidic pH will cause an underestimation of the reaction coordinate, with a 4.2% underestimation per 0.1 pH unit below pH 7.4.

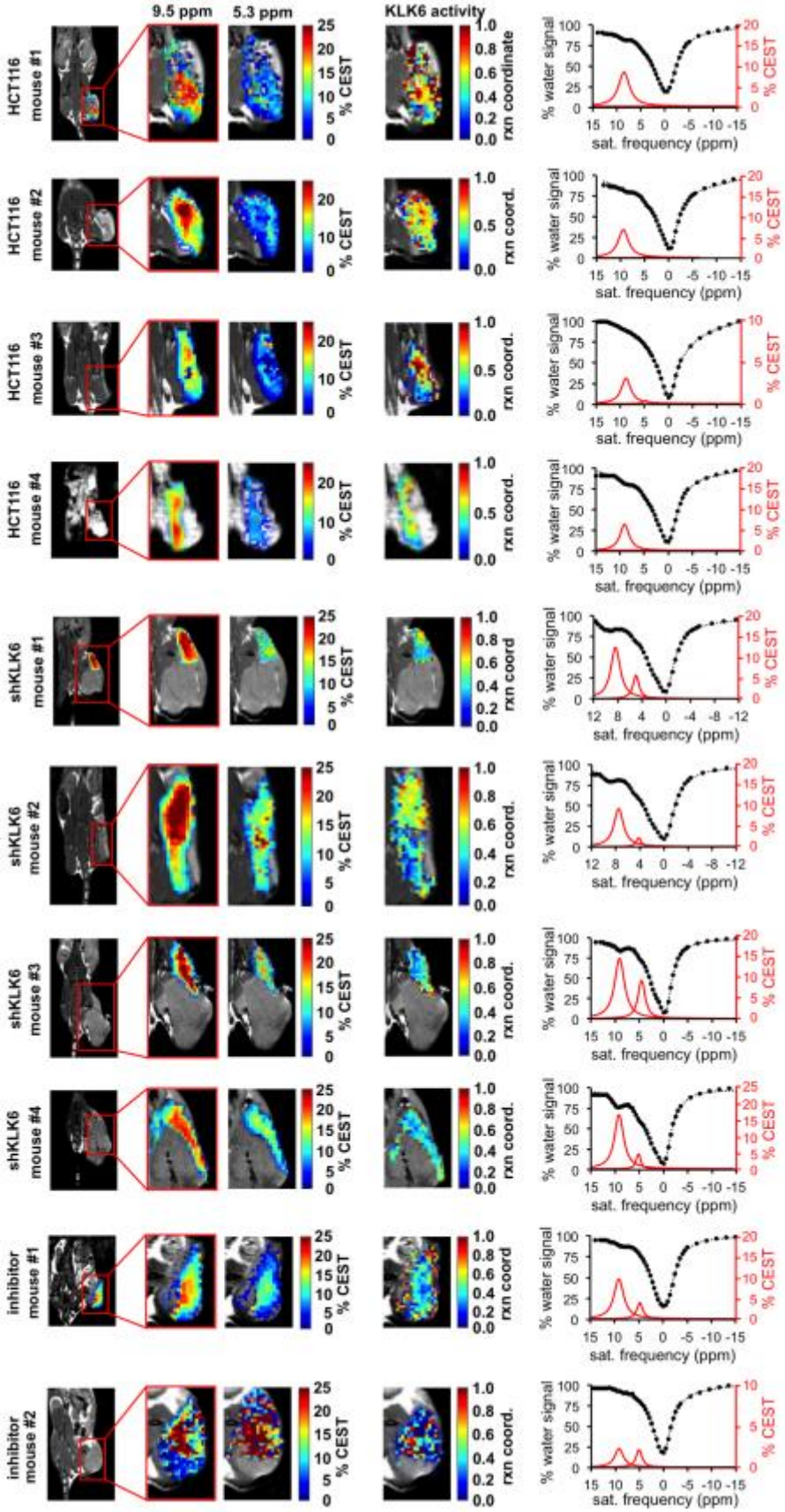
9.5 ppm
5.3 ppm
KLK6 activity
HCT116 mouse #1
HCT116 mouse #2
HCT116 mouse #3
HCT116 mouse #4
shKLK6 mouse #1
shKLK6 mouse #2
shKLK6 mouse #3
shKLK6 mouse #4
inhibitor mouse #1
inhibitor mouse #2
% CEST
rxn coordinate
rxn coord.
rxn coord
% water signal
sat. frequency (ppm)

Fig. S6 (previous page). In vivo catalyCEST MRI of all mice with a HCT116 flank tumor, a shKLK6 flank tumor, and a HCT116 flank tumor treated with Antithrombin III inhibitor. Similar results are shown in Fig. 4. **a** Anatomical images show the locations of flank tumors in each tumor model. **b** The CEST signal amplitudes in the tumors after saturation at 9.5 ppm or 5.3 ppm are overlaid on the anatomical images. **c** These CEST signal amplitudes and Eq. [2] were used to determine parametric maps of the reaction coordinates of KLK6 activity in tumor tissues. **d** CEST spectra (black) and Lorentzian line shapes (red) show the average CEST signal amplitudes within the tumors.

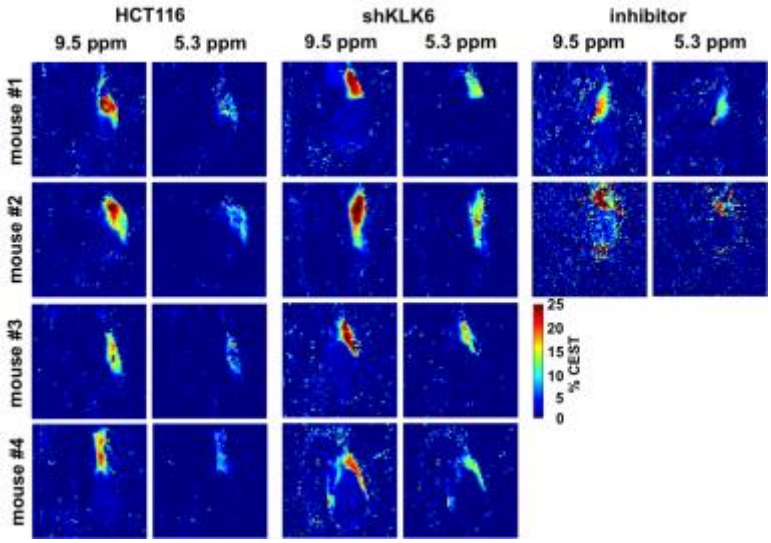

Fig. S7. Parametric maps of CEST signal amplitudes with saturation frequencies of 9.5 and 5.3 ppm for all mice with a HCT116 flank tumor, a shKLK6 flank tumor, and a HCT116 flank tumor treated with Antithrombin III inhibitor. These maps showed that the agent was not detected in regions other than the tumors.